# Simulation of microstructure evolution in fused-coating additive manufacturing based on phase field approach

**Ru-wei Geng[1], Jun Du[2], *Zheng-ying Wei[1,2] and Guang-xi Zhao[1]**

*1. State Key Laboratory for Manufacturing System Engineering, Xi'an Jiaotong University, Xi'an 710049, China*

*2. Collaborative Innovation Center of High-End Manufacturing Equipment, Xi'an 710049, China*

**Abstract:** The mechanical properties of metal components are determined by the solidification behaviour and microstructure. A quantitative phase field model is used to investigate the microstructure evolution of fused-coating additive manufacturing, by which to improve the quality of deposition. During the fused-coating process, the molten metal in a crucible flows out of a nozzle and then reaches the substrate. The solidification happens at the moment when the molten metal comes into contact with substrate moving in three-dimensional space. The macroscopic heat transfer model of fused-coating is established to get the temperature field considered as the initial temperature boundary conditions in the phase field model. The numerical and experimental results show that the morphology of grains varies with different solidification environments. Columnar grains are observed during the early period at the bottom of fused-coating layer and the equiaxed grains appear subsequently ahead of the columnar grains. Columnar dendrites phase field simulations about the grains morphology and solute distribution are conducted considering the solidification environments. The simulation results are in good agreement with experimental results.

**Key words:** phase field; microstructure evolution; fused-coating additive manufacturing

**CLC numbers:** TP391.99          **Document code:** A          **Article ID:** 1672-6421(2017)05-346-07

Metal additive manufacturing (MAM), which has developed rapidly in the past three decades, is one of a significant breakthrough in advanced manufacturing. Heat transfer, solute transportation and solidification behaviours in the process of metal solidification will affect the nucleation and growth of grains dramatically and eventually determine the microstructures of alloys. The microstructure evolution rule can be revealed clearly by combining the MAM technique with the dynamic solidification, and the relationship between the technical parameters and microstructure evolution can be discovered. Moreover, the proactive control of the microstructure and components' mechanical properties can be realized in the MAM process [1]. A review of studies in additive manufacturing development shows a significant progress in the additive manufacturing

technique [2-6]. These widely applied additive manufacturing processes include selective laser melting (SLM) [7], laser cladding (LD) [8], electron beam melting (EBM) [9], etc. Among these studies, the investigation of microstructure evolution during the AM solidification is relatively rare. The MAM usually has various process parameters, long test cycle and high cost of raw materials. Only by fully understanding the non-equilibrium solidification and microstructure evolution in the process of AM can the integration of microstructure and macroscopic mechanical properties be achieved [10]. Relying on the traditional experience and trial-error method to carry out the process research will not only have high costs, but also expend a lot of time. Phase field method is a rather prevalent method to simulate the grains growth in the solidification process. It is reliable to couple the phase field equation with other physical fields (flow field, concentration field, temperature field, etc.), and hence, the coupling of multi-physical fields will accurately describe the real process of AM.

Phase field has been used in simulating the microstructure of AM more and more extensively with

its unique advantages. V. Fallah et al [11] employed quantitative phase field model to simulate the microstructure evolution in laser powder deposition. Macroscopic numerical model was established to get the temperature gradient and the interface pulling speed [12,13]. The simulation results show that phase field model is able to be coupled with complex heat transfer model to reveal the microstructure growth in laser powder deposition. Besides, the initial temperature boundary information can also be acquired by combining the nanoscale molecular dynamics modelling with mesoscale front tracking [14]. Phase field was applied in selective laser melting (SLM) of 718 alloy [15]. Simplified heat source model was used to calculate the temperature field. Compared with the theoretical predictions of the Green equation and Kura-fisher model [16,17], grains growth of 718 alloy in steady state were verified in SLM. During the AM process, the solidification environment will determine the microstructure and therefore, the relationships between process parameters and microstructure evolution can be investigated thoroughly with the phase field method. Numerous studies have been conducted on the microstructure evolution but the experimental observations are relatively rare to verify the simulation results.

In this study, the quantitative phase field model is applied to simulate local dendrite growth in the process of fused-coating additive manufacturing. In order to get the temperature distribution in the forming process of fused-coating, macroscopic numerical calculation model of fused-coating was built. The solidification environment information, i.e., the pulling speed and temperature gradient are obtained from the macroscopic heat and mass transfer models established on the basis of fused-coating fundamental principles. The experiment was carried out on fused-coating specimen to validate the correctness of phase field model.

# 1  Modelling architecture

The fundamental principles of fused-coating are introduced to establish the macroscopic heat and flow model, which provides initial temperature boundary conditions of phase field modeling. The schematic illustration of the principle of fused-coating process is shown in Fig. 1 [18]. The metallic melt in a crucible flows out through the fused-coating channel under the applied pressure and gravity of itself. Solidification happens at the moment when the molten melt comes into contact with substrate moving in three-dimensional space. With the controlled substrate moving, the molten melt continues solidifying on the moving substrate. The solidified portion accumulates layer by
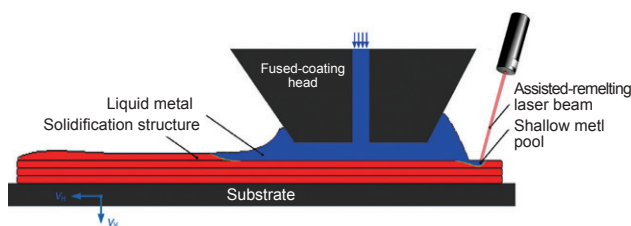


**Fig. 1:  Schematic of fused-coating additive manufacturing [18]**

layer and then the component is fabricated. A shallow melt pool comes into being under the action of assisted-remelting laser. The temperature distribution nearby the solidification front is the main information feeding into the phase field simulations, so the assisted-remelting laser is ignored in the macroscopic heat and flow modelling.

## 1.1 Macroscopic heat transfer model of fused-coating

The temperature field information can be obtained by solving the three-dimensional Fourier's heat transfer equation:

$$\frac{\partial}{\partial x}(k\frac{\partial T}{\partial x})+\frac{\partial}{\partial y}(k\frac{\partial T}{\partial y})+\frac{\partial}{\partial z}(k\frac{\partial T}{\partial z})+Q = \frac{\partial(\rho c_p T)}{\partial t}$$

where $k$ is thermal conductivity; $Q$ is the power generated per unit volume; $c_p$ (J·g$^{-1}$·k$^{-1}$) is the specific heat capacity and $\rho$(g·m$^{-3}$)  is the density of molten liquid. The initial conditions are defined as follows:

For the substrate, $T(x, y, z, t) \equiv 370$ K;

For the liquid in the fused-coating head, $T(x, y, z, t) \equiv 920$ K.

All the boundary conditions are assumed adiabatic. As for the molten liquid flowing on the substrate, volume of fluid (VOF) method is applied in this model. It was discussed in detail in Ref. [18]. Al-4.5wt.% Cu binary alloy is used for macroscopic model and the phase field simulation conditions and some thermo-physical properties are shown in Table 1.

**Table 1:  Initial condition and thermo-physical properties of Al-4.5wt.% Cu binary alloy**

| Properties | Value |
|---|---|
| Viscosity (N•s•m$^{-2}$) | 0.0013 |
| Density (kg•m$^{-3}$) | 2800 |
| Liquidus temperature (K) | 911.15 |
| Solidus temperature (K) | 775.15 |
| Latent heat of fusion (J•kg$^{-1}$) | 3.89e+05 |
| Specific heat capacity (J•kg$^{-1}$•K$^{-1}$) | 786 |
| Initial temperature of melt (K) | 920 |
| Substrate temperature (K) | 370 |
| Substrate speed (m•s$^{-1}$) | 0.1 |
| Solute diffusivity in the liquid, $D$ (m$^2$•s$^{-1}$) | 3e-9 |
| Equilibrium partition coefficient, $k$ | 0.14 |
| Anisotropy, $\varepsilon$ | 0.05 |
| Liquidus slope, $m$ [K•(wt.%)$^{-1}$] | -2.6 |
| Gibbs-Thomson coefficient, $\Gamma$(K•m) | 2.4e-7 |

## 1.2 Phase field model

The quantitative phase field model [19] is employed to simulate dendrite structure of fused-coating process. The dimensionless concentration $U$ is defined as

$$U = \frac{\exp(\mu)-1}{1-k}$$

and

$$\mu = \ln(\frac{2c/c_\infty}{1+k-(1-k)\phi})$$

where $k$ is the equilibrium partition coefficient; $c$ is the solute concentration of binary alloy; $C_\infty$ is the concentration far from the interface; $\phi$ is the order parameter which is +1 in solid and -1 in liquid. Ignoring the convention in the molten melt during the solidification process, the phase field equations can be expressed as [20]:

$$\tau \frac{\partial \phi}{\partial t} = W^2 \nabla^2 \phi + \phi - \phi^3 - \lambda g'(\phi)(\theta + Mc_\infty U)$$

$$\left(\frac{1+k}{2} - \frac{1-k}{2}\phi\right)\frac{\partial U}{\partial t} = \nabla \left( Dq(\phi)\nabla U + \frac{1}{2\sqrt{2}}\left[1+(1-k)U\right] \times \frac{\partial \phi}{\partial t}\frac{\nabla \phi}{|\nabla \phi|}\right)$$
$$+\left[1+(1-k)U\right]\frac{1}{2}\frac{\partial \phi}{\partial t}$$

$$\frac{\partial \theta}{\partial t} = \alpha \nabla^2 \theta + \frac{1}{2}\frac{\partial \phi}{\partial t}$$

where $\lambda$ is the coupling constant; $M$ is the scaled magnitude of the liquidus slope $M = \frac{-m(1-k)}{L/c_p}$; $\theta$ is dimensionless undercooling; $W$ is the width of the diffuse interface; $\tau$ is the relaxation time; $D$ is the solution diffusivity in the liquid; $\alpha$ is thermal diffusivity; $q(\phi) = \frac{1-\phi}{2}$ and $g'(\phi) = (1-\phi^2)^2$.

In the process of fused-coating, temperature gradient would be produced near the solid/liquid interface on the relative cool substrate. The temperature field equation of this micro domain can be defined as:

$$T(z,t) = T_0 + G(t)(Z - Z_0 - \int_0^t V_p(t')dt')$$

where $T$ is the tmperature of the phase field simulation domain; $T_0$ is the reference temperature; $z$ is the coordinates perpendicular to the S/L interface direction; $G$ is the temperature gradient; $V_p$ is the solidification speed; $t$ is time, and $T(z_0,0)=T_0$; taking into account this equation above and the temperature-dependent relaxation time $\tau = \tau_0[1-(1-k)(z-V_pt)/l_T]$ [21], the final set of equations is

$$\tau[1-(1-k)\frac{Z-\int_0^t V_p(t')dt'}{l_T}]\frac{\partial \phi}{\partial t} = W^2\nabla^2\phi + \phi - \phi^3 - \lambda g'(\phi)(U + \frac{Z-\int_0^t V_p(t')dt'}{l_T})$$

$$\left(\frac{1+k}{2} - \frac{1-k}{2}\phi\right)\frac{\partial U}{\partial t} = \nabla \left( Dq(\phi)\nabla U + \frac{1}{2\sqrt{2}}\left[1+(1-k)U\right] \times \frac{\partial \phi}{\partial t}\frac{\nabla \phi}{|\nabla \phi|}\right)$$
$$+\left[1+(1-k)U\right]\frac{1}{2}\frac{\partial \phi}{\partial t}$$

where $l_T = |m|(1-k)c_\infty/kG$; $m$ is the liquids slope of the dilute alloy phase diagram. The relationship of phase field parameters can be acquired from the thin-interface limit analysis [22]

$$W = \frac{d_0\lambda}{a_1}$$

and

$$\tau = \frac{a_2\lambda}{D}W^2$$

where the capillary length $d_0 = \Gamma/\Delta T$, $\Gamma = \sigma T/L$ is the Gibbs-Thomson coefficient; $\sigma$ is the interfacial free energy; $D$ is the solution diffusivity in the liquid; $\Delta T = [|m|(1-k)c_\infty]/k$,

$a_1 = 0.8839$, $a_2 = 0.6267$ [23].

The quantitative phase field model is employed to reveal the dendrite growth during the fused-coating process. The phase field parameters, i.e., dimensionless undercooling, temperature gradient, solidification velocity, can be obtained from the macroscopic heat and flow transfer models. The temperature gradient $G$ at the bottom of the melt pool near the fusion line can be defined as $G = (T_p-T_l)/d$, where $T_p$ is the highest temperature and $T_l$ is the lowest temperature in the selected phase field calculating zone near the fusion line; $d$ is the distance between $T_p$ and $T_l$. The relationship between solidification speed $v_p$ and fused-coating speed $v$ is $v_p = v\cos\alpha$, where $\alpha$ is the angle between fused-coating direction and dendrite growth direction. The dendrites grow along the direction of temperature gradient, namely perpendicular to the isotherm.

# 2 Results and discussion

## 2.1 Macroscopic fused-coating simulation

The temperature distribution in the melt pool is the major research intent in this section. Some phase field parameters, i.e., thermal gradient $G$, solidification speed $V_p$, are extracted from these fused-coating simulations. Al-4.5wt.% Cu is used in the macroscopic and micro simulations.

Figure 2 shows the temperature distribution of fused-coating process at 0.2 s, 0.4 s, 0.6 s, 0.8 s and 1.0 s, respectively. Solidification process started from the molten metal with high temperature coming into contact with cold substrate. The molten metal cools dramatically and the temperature goes down below the liquidus under the cooling influence of substrate. With time goes on, the solid-liquid interface evolves gradually as shown in Fig. 2(b)–2(e), and eventually gets a relative stable stage. The temperature gradient $G$ can be extracted from a micro-domain in Fig. 2(e). It is assumed that the temperature gradient $G$ keeps constant in the calculation domain of phase field and $G = (T_p - T_l)/d$, where $T_p$ is the highest temperature in the micro-domain marked in Fig. 2(e) and $d$ is the distance from $T_p$ to $T_l$. The changing curve of temperature vs distance from $T_p$ to $T_l$ at the bottom of fused-coating layer is shown in Fig. 3.

In the phase field theory, the order parameter $\phi$ is used to symbolize the material state, where $\phi =1$ for solid and $\phi =-1$ for liquid. When the value of $\phi$ is between -1 and 1, it is the solid-liquid interface. Similarly, solid fraction is employed here to indicate the state of molten metal. The solid fraction of 0.5 is regarded as the solid-liquid interface when the dendrite growth direction is investigated. In this way, the moving speed of interface can be calculated by [24]:

$$V_p = V\cos\alpha$$

where $V$ is the relative velocity between fused-coating head and substrate; $\alpha$ is the angle between the normal to the interface and the relative speed direction.

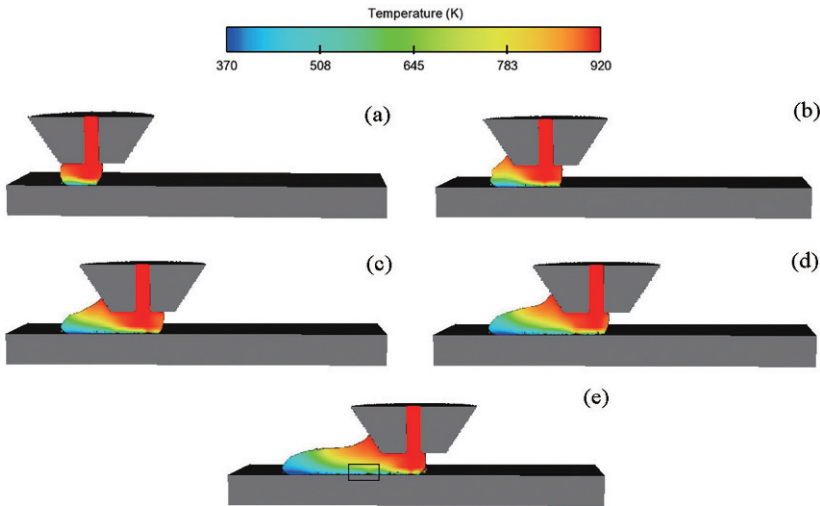Figure 4 shows the solid fraction distribution in fused-coating layer.

**Fig. 2:** Simulated temperature field viewed from center-plane longitudinal section of fused-coating process at 0.2 s, 0.4 s, 0.6 s, 0.8 s, 1.0 s, respectively
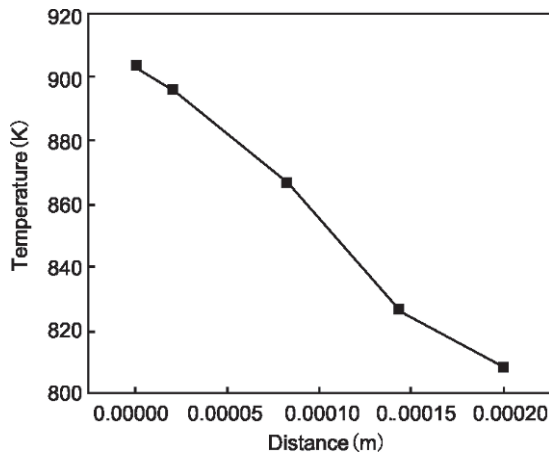


**Fig. 3:** Changing curve of temperature vs. distance from $T_P$ to $T_l$ at bottom of fused-coating layer
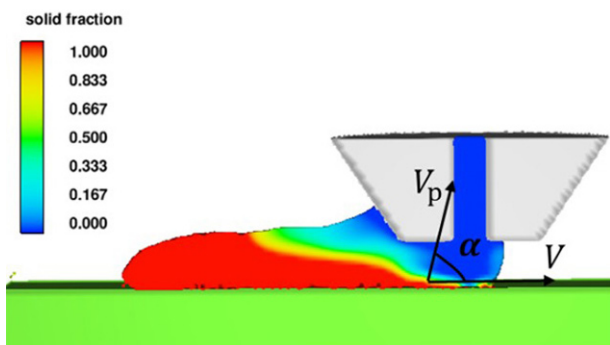


**Fig. 4:** Solid fraction distribution in fused-coating layer

## 2.2 Microstructure evolution

By combining the solidification environment at the bottom of melt pool into the phase field model, the microstructure evolution and solute distribution are obtained. The evolution of dendrite patterns simulated by phase field at the bottom of melt pool is shown in Fig. 5. The initial condition is a thin solid layer at the bottom of simulation domain. In the first stage of microstructure evolution (Fig. 5a), the solid/liquid (S/L) interface becomes fluctuated and lots of small

grains branch advancing into the liquid. With the solidification continuing, the Cu element of Al-4.5wt.%Cu alloy diffuses in the direction of the advancing interface and then the solute enrichment in the front of interface is obvious. The temperature gradient is perpendicular to the S/L interface, and the grains grow up gradually along the temperature gradient and meanwhile, the competitive growth stage occurs [Fig. 5(b)]. But the grain size is different with each other. Only a few grains can survive from this stage and become the primary dendrites [Fig. 5(c)]. The primary dendrites arm space increases and the solute enrichment is more obvious. The dendrites continue to growing up along the direction of temperature gradient $G$ at the solidification velocity $V_p$. But the relative small dendrites among the primary dendrites shrink slowly in this process [Fig. 5(c)–5(d)]. In the last stage [Fig. 5(d)], the primary dendrite arm space and the amount of grains almost keep constant and the growth patterns turn into a relative stable stage.

The solute distribution is a crucial issue in studying the solidified microstructure. The solution segregation, which has great influences on mechanical properties, is a typical phenomenon happening in the solidification process. In order to research the solute distribution, the concentration field at 1.0 s is shown in Fig. 6(a). Three lines are selected in the concentration field to investigate the solution distribution along them. The results of solute distribution along the selected lines are shown in Fig. 6(b) to 6(d), respectively. It should be noted that the concentration here is the relative concentration, i.e. the ratio of $c$ to $c_\infty$. Figure 6(b) depicts the solution distribution between two primary dendrites along A-A'. The value of relative concentration in the liquid is 1 and increases significantly to about 1.7 when it reaches the zone between the two primary dendrites. It is because the Cu element of the Al-Cu alloy diffuses to the liquid between two primary dendrites, which is located in enclosed or semi-enclosed areas. So the Cu element cannot diffuse sufficiently. Figure 6(c) represents the concentration through the primary dendrite. There is a sharp concentration increase in the area close to the interface from the liquid side, and immediately the concentration decreases rapidly when it enters the solid phase. The reason is that solute enrichment happens near the S/L interface, other than the places between the two adjacent dendrites, the solute near the dendrite tip is able to diffuse sufficiently in time and space. Figure 6(d) describes the solute distribution perpendicular to the dendrite growth direction. It is apparent that the concentration between the two adjacent dendrites is much higher than the concentration inside the column dendrites. With the growth of dendrites, there is no time and space for solute to diffuse and consequently the micro segregation occurs.
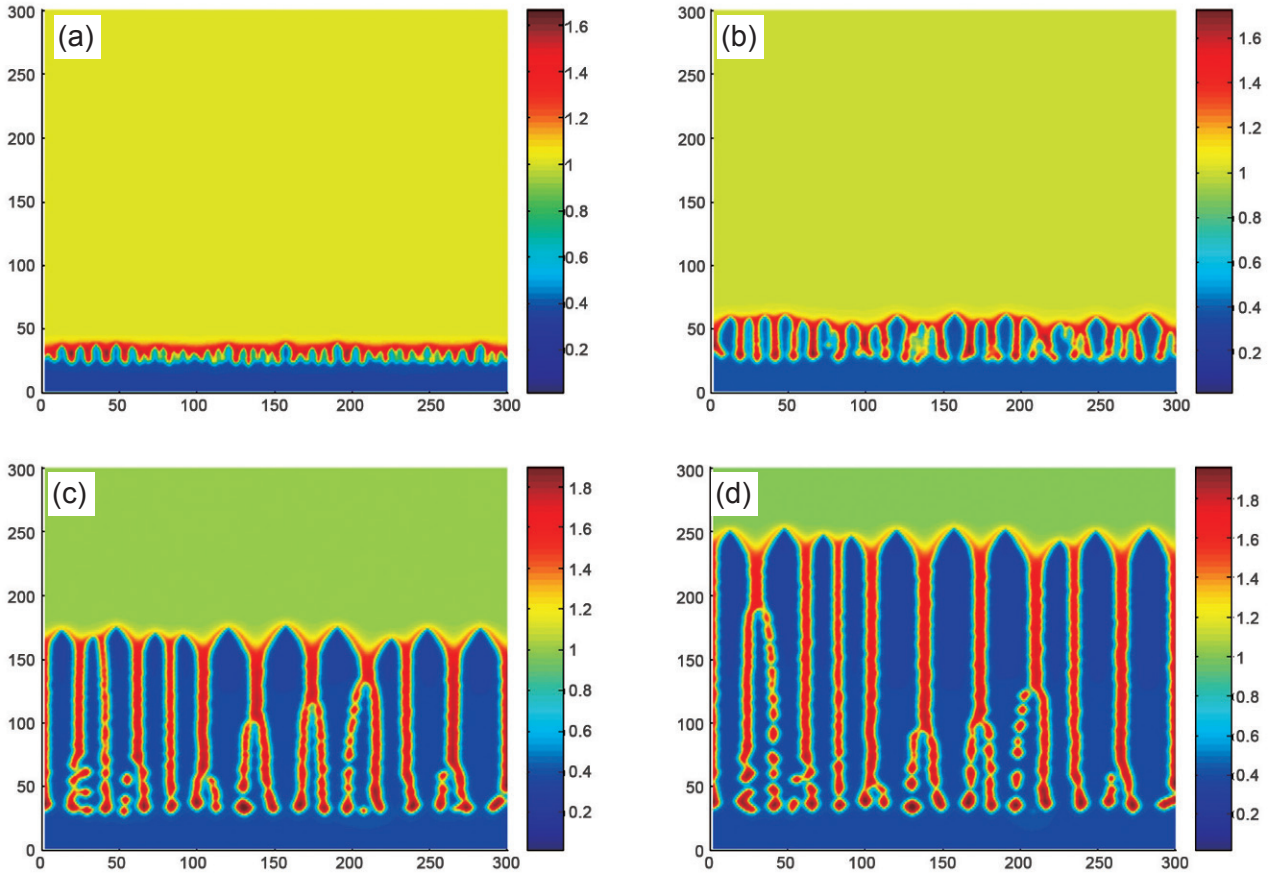
Fig. 5: Microstructure evolution at bottom of melt pool. The *x*-axis and *y*-axis values are number of grids in phase field simulations, which means 300×300 grids throughout entire domain
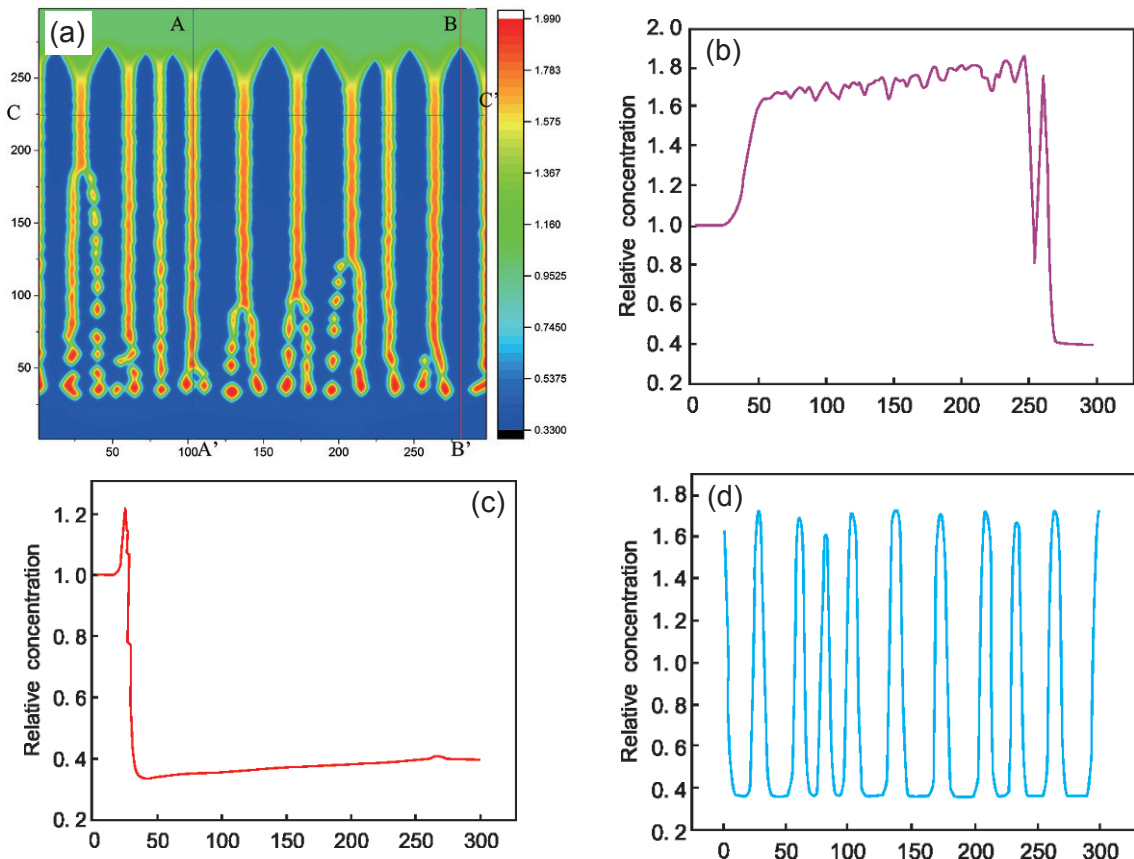


Fig. 6: Concentration field at 1.0 s (a) and solute distribution contour along A-A' (b), concentration along B-B' (c) and concentration along C-C' (d)

# 3 Experiment validation

Metallographic examination was carried out on fused-coating specimen in order to validate the phase field model. Figure 7 shows the comparisons of the microstructures between phase field simulations and experimental observations. The experimental results reveal the microstructure from a cross-section of fused-coating layer parallel to the forming direction [Fig. 7(a)]. The columnar dendrites growing along the direction of temperature gradient can be seen at the bottom of fused-

coating layer. Because of the random disturbances in the solidification process, the morphology of dendrites presents nonlinear characteristics which are consistent with phase field simulations in Fig. 7(b). According to the experimental results, the sizes of columnar crystals are different from each other. There are a few of columnar dendrites marked in Fig. 7(a), which are much smaller than the primary dendrites. This phenomenon also can be observed in the simulations. The reason for this phenomenon is that the crystals compete with each other in the growth process.
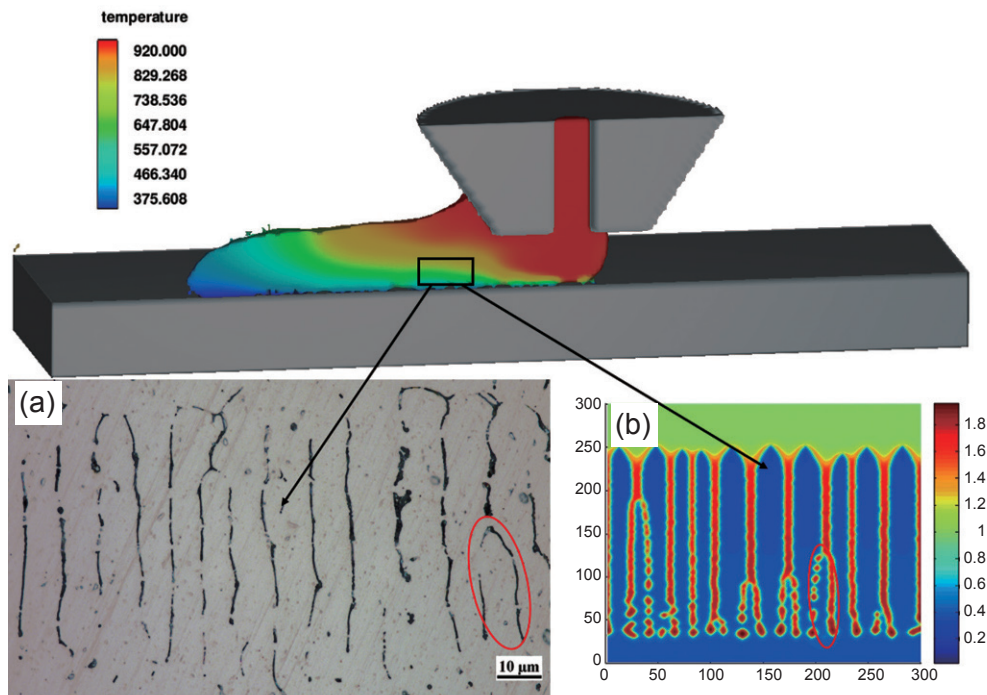


**Fig. 7: Microstructure at bottom of fused-coating layer: (a) experimental result under microscope, (b) phase field simulation result**

In the early stage of solidification, the molten melt with high temperature (920 K) flows out of the fused-coating head and reaches the substrate with a relative low temperature (370 K). The solidification starts at the interface between melt and substrate at the moment of the melt contacts with the substrate. The upper melt has no time to cool at this moment and the temperature of which is still very high. Consequently, under the effect of temperature gradient, the columnar dendrites form at the bottom of fused-coating layer (Fig. 8). With the cooling and solidification continuing, the temperature of upper part melt decreases to lower than the melting point. The nuclei are created in the supercooling liquid and grow up in different directions, and finally the equiaxed grains can be seen above the columnar grains. Figure 8 describes the columnar-to-equiaxed transition (CET) in the fused-coating layer. The columnar dendrites grow upwards from the bottom of fused-coating layer. In the subsequent solidification process, the equiaxed grains grow up in random directions ahead of the columnar zone and therefore, the growth of columnar front is inhibited by the equiaxed grains.
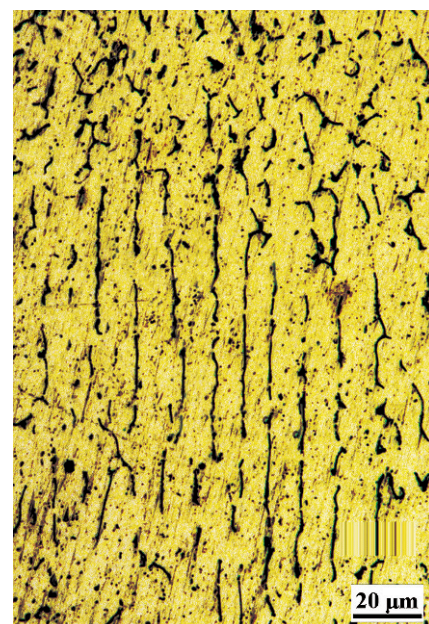


**Fig. 8: Columnar-to-equiaxed transition (CET) in fused-coating layer**

# 4  Conclusions

The quantitative phase field model was employed to simulate the microstructure evolution of fused-coating additive manufacturing. In order to get the temperature distribution in the forming process of fused-coating, macroscopic numerical calculation model of fused-coating was built. Additionally, the metallographic examination of fused-coating specimen was carried out with the purpose of validating the microstructure simulations.

The temperature distribution and other thermal boundary conditions were extracted from the fused-coating numerical calculation model. According to the simulations and experimental results, the columnar dendrites were formed at the bottom of fused-coating layer under the effect of temperature gradient. With the solidification continuing, equiaxed grains were formed in the upper part of the fused-coating layer. Moreover, the columnar-to-equiaxed transition (CET) can be observed from metallographic examination. The dendrite growth and solution distribution were revealed by using quantitative phase field model. The closer it is to the interface from the liquid side, the higher the concentration. The solute segregation in the solidification process was also illustrated by extracting the solute concentration among columnar dendrites.

The microstructure evolution at the bottom of fused-coating layer was obtained by quantitative phase field model, which is in accordance with the results obtained by optical microscope. Therefore, the solidified microstructure can be simulated correctly by phase field method in the fused-coating process.

# References

[1]  Wang Huaming. Materials' fundamental issues of laser additive manufacturing for high-performance large metallic components. Acta Aeronautica et Astronautica Sinica, 2014, 35(10): 2690–2698. (In Chinese)

[2]  Arcella F G, Froes F H. Producing titanium aerospace components from powder using laser forming. JOM, 2000, 52(5): 28–30.

[3]  Gong Shuili, Suo Hongbo, Li Xuehuai. Development and Application of Metal Additive Manufacturing Technology. Aeronautical Manufacturing Technology, 2013, 13: 66. (In Chinese)

[4]  Wilkes J, Hagedorn Y C, Meiners W. Additive manufacturing of $ZrO_2$-$Al_2O_3$ ceramic components by selective laser melting. Rapid Prototyping Journal, 2013, 19(1): 51–57.

[5]  Heinl P, Rottmair A, Korner C. Cellular titanium by selective electron beam melting. Advanced Engineering Materials, 2007, 9(5): 360–364.

[6]  Yan Yongnian, Qi Haibo, Lin Feng, et al. Produced Three-dimensional Metal Parts by Electron Beam Selective Melting. Chinses Journal of Mechanical Engineering, 2007, 43(6): 87. (In Chinese)

[7]  Brandl E, Heckenberger U, Holzinger V, et al. Additive manufactured AlSi10Mg samples using Selective Laser Melting (SLM): Microstructure, high cycle fatigue, and fracture behavior. Materials & Design, 2012, 34: 159–169.

[8]  Fallah V, Corbin S F, Khajepour A. Process optimization of Ti–Nb alloy coatings on a Ti-6Al-4V plate using a fiber laser and blended elemental powders. Journal of Materials Processing Technology, 2010, 210(14): 2081–2087.

[9]  Chao Yanpu, Qi Lehua, Zuo Hansong, et al. Remelting and bonding of deposited aluminum alloy droplets under different droplet and substrate temperatures in metal droplet deposition manufacture. International Journal of Machine Tools & Manufacture, 2013, 69(3): 38–47.

[10]  Lin Xin, Yang Haiou, Chen Jing, et al. Microstructure Evolution of 316L Stainless Steel During Laser Rapid Forming. Acta Metallurgica Sinica, 2006, 42(4): 361–368.

[11]  Fallah V, Amoorezaei M, Provatas N, et al. Phase-field simulation of solidification morphology in laser powder deposition of Ti-Nb alloys. Acta Materialia, 2012, 60(4):1633–1646.

[12]  Fallah V, Corbin S F, Khajepour A. Process optimization of Ti-Nb alloy coatings on a Ti-6Al-4V plate using a fiber laser and blended elemental powders. Journal of Materials Processing Technology, 2010, 210(14): 2081–2087.

[13]  Fallah V, Alimardani M, Corbin S F, et al. Temporal development of melt-pool morphology and clad geometry in laser powder deposition. Computational Materials Science, 2011, 50(7): 2124–2134.

[14]  Xie Yu, Dong Hongbiao, Liu Jun, et al. A Multi-Scale Approach to Simulate Solidification Structure Evolution and Solute Segregation in a Weld Pool. Journal of Algorithms & Computational Technology, 2013, 7(4): 489–508.

[15]  Kundin J, Mushongera L, Emmerich H. Phase-field modeling of microstructure formation during rapid solidification in Inconel 718 superalloy. Acta Materialia, 2015, 95:343–356.

[16]  Kouchair S. Weld Metal Chemical Inhomogeneities. Welding Metallurgy, Second Edition. John Wiley & Sons, Inc. 2003, Chapter 10: 243–262.

[17]  Poorhaydari K, Patchett B M, Ivey D G. Estimation of cooling rate in the welding of plates with intermediate thickness. Welding Journal, 2005, 84(10): 149s–155s.

[18]  Jun Du, Zhengying Wei, Xin Wang, et al. A novel high-efficiency methodology for metal additive. Appl. Phys. A, 2016, 122(11): 945.

[19]  Ramirez J C, Beckermann C, Karma A, et al. Phase-field modeling of binary alloy solidification with coupled heat and solute diffusion. Physical Review E Statistical Nonlinear & Soft Matter Physics, 2004, 69(1): 051607.

[20]  Karma A. Phase-field formulation for quantitative modeling of alloy solidification. Physical Review Letters, 2001, 87(11):115701.

[21]  Echebarria B, Folch R, Karma A, et al. Quantitative phase-field model of alloy solidification. Physical Review E Statistical Nonlinear & Soft Matter Physics, 2004, 70(1): 061604.

[22]  Echebarria B, Folch R, Karma A, et al. Quantitative phase-field model of alloy solidification. Physical Review E Statistical Nonlinear & Soft Matter Physics, 2004, 70(1): 061604.

[23]  Karma A, Rappel W J. Quantitative phase-field modeling of dendritic growth in two and three dimensions. Physical Review E, 1998, 57(4): 4323–4349.

[24]  Zimmermann M, Carrard M, Kurz W. Rapid solidification of Al-Cu eutectic alloy by laser remelting. Acta Metallurgica, 1989, 37(12): 3305–3313.